

## **A NOVEL WIDEBAND CIRCULARLY POLARIZED ANTENNA FOR WORLDWIDE UHF BAND RFID READER APPLICATIONS**

**E. Mireles and S. K. Sharma\***

Antenna and Microwave Laboratory, Department of Electrical and Computer Engineering, San Diego State University, 5500 Campanile Drive, San Diego, CA 92182-10309, USA

**Abstract**—This paper presents the novel design of a wideband circularly polarized (CP) Radio Frequency Identification (RFID) reader microstrip patch antenna for worldwide Ultra High Frequency (UHF) band which covers 840–960 MHz. The proposed antenna, which consists of a microstrip patch with truncated corners and a cross slot, is placed on a foam substrate ( $\epsilon_r = 1.06$ ) above a ground plane and is fed through vias through ground plane holes that extend from the quadrature 3 dB branch line hybrid coupler placed below the ground plane. This helps to separate feed network radiation, from the patch antenna and keeping the CP purity. The prototype antenna was fabricated with a total size of  $225 \times 250 \times 12.8 \text{ mm}^3$  which shows a measured impedance matching band of 840–1150 MHz (31.2%) as well as measured rotating linear based circularly polarized radiation patterns. The simulated and measured 3 dB Axial Ratio (AR) bandwidth is better than 23% from 840–1050 MHz meeting and exceeding the target worldwide RFID UHF band.

### **1. INTRODUCTION**

The use of radio frequency (RF) signals to identify objects is a practice that has been employed since World War I. However, back in those days, implementation of such devices was limited to specific applications due to high cost and big size of RF components. In today's day to day life, Radio Frequency Identification (RFID) technology has seen significant growth mainly due to invent of low cost compact solid state devices. The antennas for RFID systems also play a crucial

---

*Received 10 May 2012, Accepted 19 June 2012, Scheduled 25 June 2012*

\* Corresponding author: Satish Kumar Sharma (ssharma@mail.sdsu.edu).

role in the continuous development of this technology. Antennas are utilized both in the process of transmitting/receiving an RF signal at the interrogator and at the object to be identified, namely reader and tag antennas, respectively. Since the purpose of the reader antenna is to track down the presence of one or several tag antennas, which are normally linearly polarized, no matter their orientation, circular polarization (CP) radiation at the reader side is preferred in order to make the process of identification reliable and thus more efficient [1, 2]. The CP radiation can be generated by having two linearly polarized electric field components of equal magnitude, and forming right angle with  $90^\circ$  time phase difference. The relation in phase between these two components determines the sense of rotation (right or left handed) while the axial ratio (AR) describes the relationship in between the magnitude of the components which sets the CP purity achieved [3–5]. RFID technology in the ultra-high frequency (UHF) band has a specific frequency allocation designated for each country. The United States Federal Communications Commission (FCC) designates 902–928 MHz band, the European Union Nations allows the usage of 865–868 MHz band while Japan permits a band of 952–954 MHz. Recently, China approved 840.25 to 844.75 MHz for this application. Thus, the entire world wide RFID band frequency range is from 840–960 MHz [6–8].

Interesting broadband antennas for RFID fixed applications in the UHF band and the ISM band (2.4–2.8 GHz) have been reported in the literature, such as in [9], which need either elaborate feeding structure, low loss material, or stacked layers to improve impedance matching and AR bandwidths. This adds to antenna complexity and hence costly fabrication process. In addition to this, some other antenna designs that exhibit good wideband behavior, are still not able to meet the entire UHF RFID band either as AR bandwidth, or impedance matching bandwidth [10], or both [11] while maintaining a similar or even twice the volume occupied than the proposed antenna in this paper. Table 1 ([10, 11] and [12–16]) compares recent broadband RFID reader antennas for the use in the UHF band. It specifies the antenna performance in terms of impedance matching, axial ratio (AR), CP gain, and 3-dB AR beamwidth as discussed in the literature. It also contrasts the antenna geometry employed to generate expected performance results against the one proposed in this work.

In this paper, a novel circularly polarized RFID reader antenna with wide AR and impedance matching bandwidths covering the worldwide UHF band (840–960 MHz) is proposed. Please note throughout the paper, highlighted band is from 860 to 960 MHz (old worldwide UHF band) only and does not highlight the new extension from 840.25 to 844.75 MHz. The proposed antenna structure consists



of a single layer microstrip patch with truncated corners on foam substrate and a 3dB quadrature branch line coupler as the feed network [20]. These have shown generation of CP in [10, 12, 14, 16], and [17–19]. The novelty of the antenna structure is in the way, the patch is excited by employing vias through ground plane holes and connected to the branch line hybrid coupler in addition to the patch geometry. This helps to separate feed network radiation from the patch antenna and maintains the CP purity. A cross slot is mainly added to achieve compactness as reported in [21]. In regards to a wideband CP patch, AR bandwidth of 33% is reported in [22] but with the help of stacked antenna geometry. The quadrature feed network gives  $90^\circ$  out of phase currents that feeds the patch and controls having right or left-handed CP radiation when feeding through alternate ports. Since the hybrid coupler is an isolated feed geometry, unwanted radiation that may be generated due to power reflected from an antenna mismatch at the output ports is absorbed by the match terminated port which helps to achieve a good AR performance [23]. The use of such a feeding technique for UHF RFID reader antenna applications has been reported in [12] achieving a wideband performance by means of stacked microstrip patches. A CP radiation pattern has also been accomplished by using the hybrid coupler to feed two orthogonally-placed linearly polarized antennas [24]. According to [17], this type of configuration exhibits rapid degradation of the CP as moving away from the broadside ( $\theta = \Phi = 0^\circ$ ) position. RFID reader antennas with similar dimensions but covering a single UHF band designated for this technology have also been recently reported [25, 26]. Next Section presents the antenna geometry and simulation results including important parametric study results. Experimental verification of this antenna is discussed in Section 3. Section 4 presents conclusion of the work.

## 2. ANTENNA GEOMETRY AND SIMULATION RESULTS

### 2.1. Antenna Design Parameters

The proposed reader antenna consists of a square patch of dimension  $154\text{ mm} \times 154\text{ mm}$  which is suspended  $h = 11.2\text{ mm}$  above a ground plane of size  $225\text{ mm} \times 250\text{ mm}$  on a Cuming foam substrate ( $\epsilon_r = 1.06$ ,  $\tan \delta = 0.002$ ). The patch is fed at two points using vias which connects it to a  $90^\circ$  out of phase output ports of a 3 dB branch line hybrid coupler that is printed on the bottom side of the ground plane substrate (FR4,  $\epsilon_r = 4.4$ ,  $\tan \delta = 0.02$ ). The vias extend from the feed network to the patch through circular holes on the ground plane. The hybrid

helps the patch antenna to generate Right Hand Circular Polarization (RHCP) or Left Hand Circular Polarization (LHCP) based on which port between the ports 1 and 4 is selected as the input port. The feed network is separated from the antenna layer by the ground plane which helps to separate the feed network radiation, from the patch antenna and thus maintains the CP purity. Figure 1 shows the proposed antenna geometry. The coordinates of the feed points among the patch are specified in this figure with respect to center of the square patch. Size of the truncation of the corners along  $y$ -axis is 15 mm from the tip of the corner. The antenna geometry is symmetric along  $y$ -axis and has an overall size of  $225 \times 250 \times 12.8 \text{ mm}^3$ . Some preliminary results of this antenna were presented in [27].

The patch has truncated corners for enhancing the AR bandwidth and a cross slot is placed at the center of the square patch which is symmetric to the  $y$ - and  $x$ -axes mainly helping to achieve compactness in the antenna design and tuning the bandwidth. Proper combination and implementation of above mentioned techniques helps to achieve a wide AR and impedance matching bandwidths while maintaining a single layer patch design. The quadrature power divider is placed below the ground plane, hence it separates the antenna from the feed network and can be combined with RF circuit components. It also

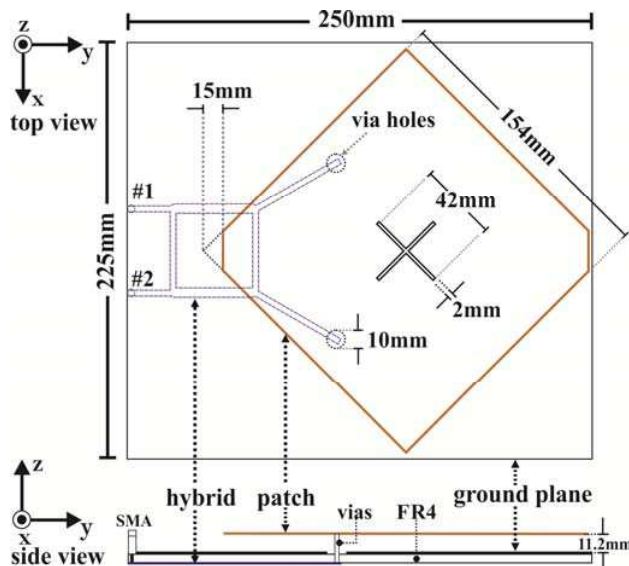


**Figure 1.** Proposed RFID reader microstrip patch antenna geometry along with feed network on the backside of the ground plane.

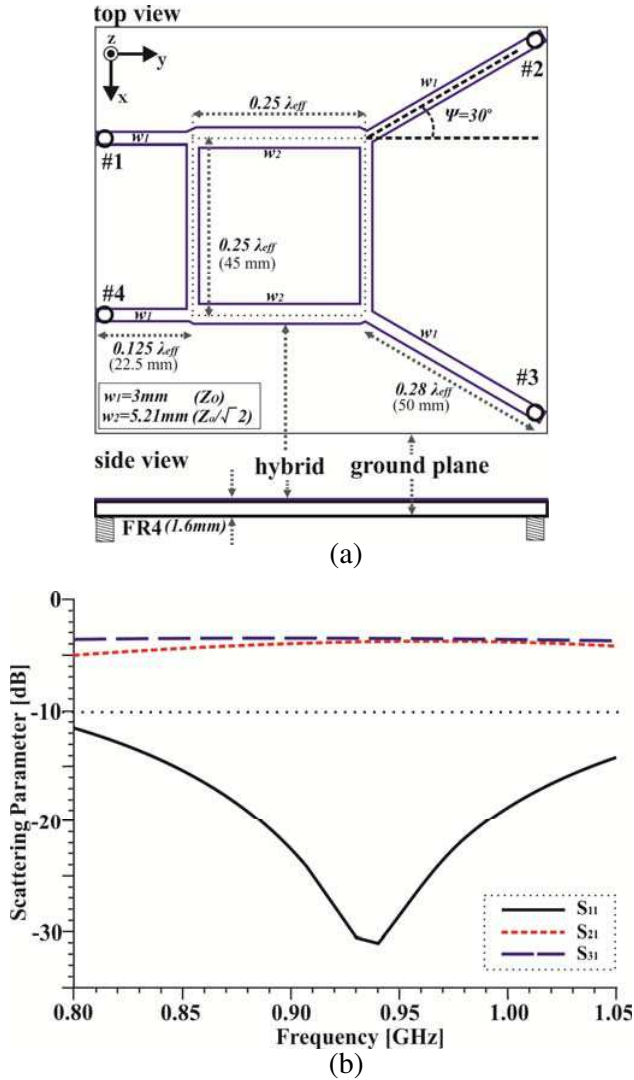


**Figure 2.** (a) Antenna design parameter dimensions and (b) simulated scattering parameters vs. frequency (GHz) of the proposed feed network.

helps in maintaining the patch radiation pattern purity. The vias help to connect the feed network outputs to the patch. Combining these techniques to achieve wide bandwidth performance while maintaining low profile is possible due to incorporation of the via holes in the ground



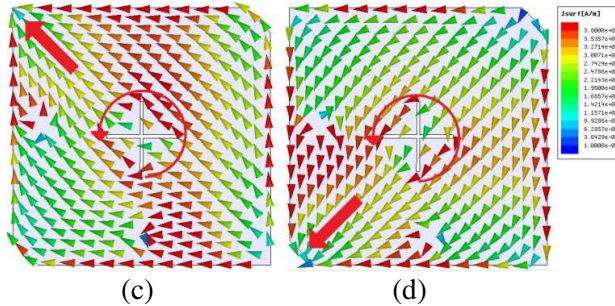


**Figure 3.** Surface current distributions at 910 MHz for four different phase intervals: (a)  $0^\circ$ , (b)  $90^\circ$ , (c)  $180^\circ$ , and (d)  $270^\circ$ .

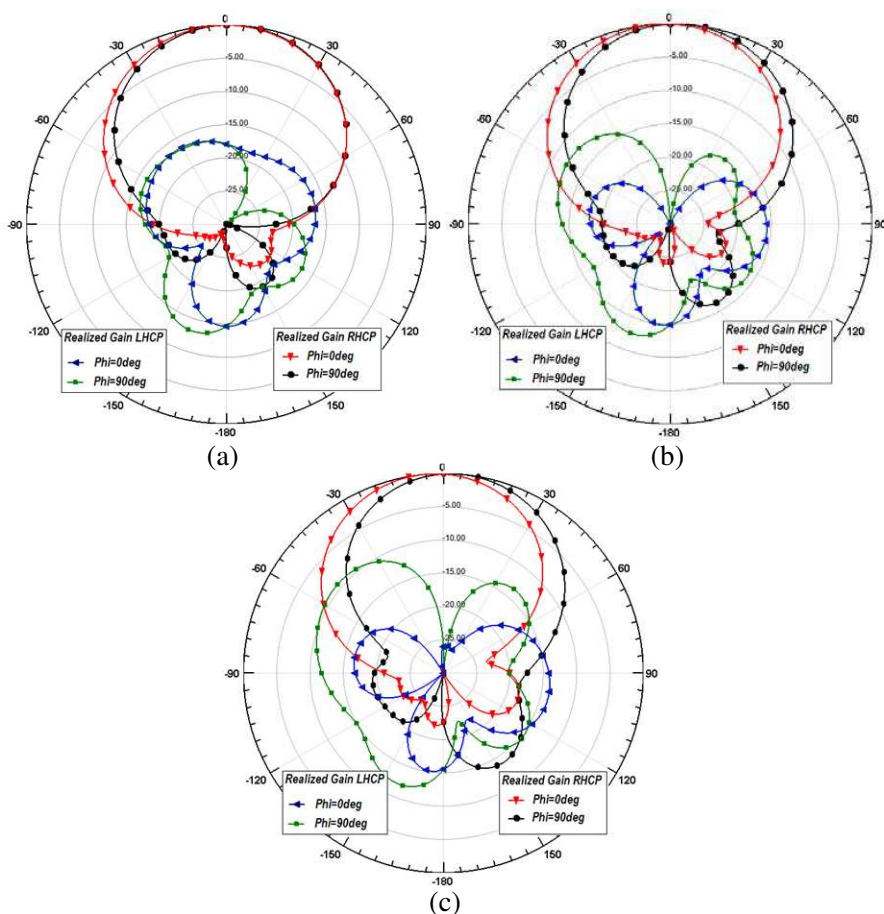
### 2.3. Simulated Radiation Patterns

Figure 4 shows the normalized simulated CP radiation patterns at 860 MHz, 910 MHz, and 960 MHz within the UHF frequency band. It can be seen that around 15 dB front-to-back (F/B) ratio is achieved at these frequencies. The co-polarization RHCP patterns are symmetric at all the frequencies. The maximum cross-polarization LHCP radiation patterns are separated from the co-polarization ones by almost 10 to 16 dB. The 3 dB beamwidths are around  $60^\circ$  which suggests wide angular coverage for the reader antenna. The maximum RHCP gain varies between 8 dBic and 5 dBic within the UHF band, where the best gain is happening towards middle of the band. Thus the pattern behavior is almost consistent throughout the band which is a desired feature for a RFID reader antenna.

### 2.4. Parametric Study Results

This section is intended to give an insight into some of the design parameters considered in this antenna. The parameters considered are the ground plane size, the width and length of the cross slot, radius of the via holes in the ground plane, the truncation of the corners in the patch, and height of the patch, radius of the via holes in the ground plane, and the angle  $\Psi$  specified in Figure 2(a) and the length of the output arms of the 3 dB coupler. In order to clearly visualize the effect on the antenna behavior for each of them, every graph shown below exhibits the variation of only one of the parameters while others are kept constant. The solid line indicates the final simulation result for all of the graphs presented. The highlighted area of the graphs represents the UHF RFID band of interest (860–960 MHz) before the recent addition of the China's RFID band from 840.25 to 844.75 MHz.

The first parameter investigated is the ground plane size (Figure 5). As mentioned previously, the proposed dimensions are 225 mm × 250 mm which yields a surface area of 562.5 cm<sup>2</sup>. An increase of this area has a minor effect in the matching band performance since the criteria  $S_{11} \leq -10$  dB is well maintained over the entire band of interest with a bandwidth of ~ 30% (final simulated design covers 828 to 1134 MHz) while a slight shift down in frequency is produced as the surface area is increased. The 255 mm × 280 mm case, which is the largest one studied, shifts the matching band down to 825–1132 MHz (Figure 5(a)). The AR response is mainly affected at the higher end of the band as the ground plane size increases while the lower end remains



**Figure 4.** Simulated normalized CP radiation patterns within UHF band frequencies: (a) 860 MHz, (b) 910 MHz, and (c) 960 MHz.

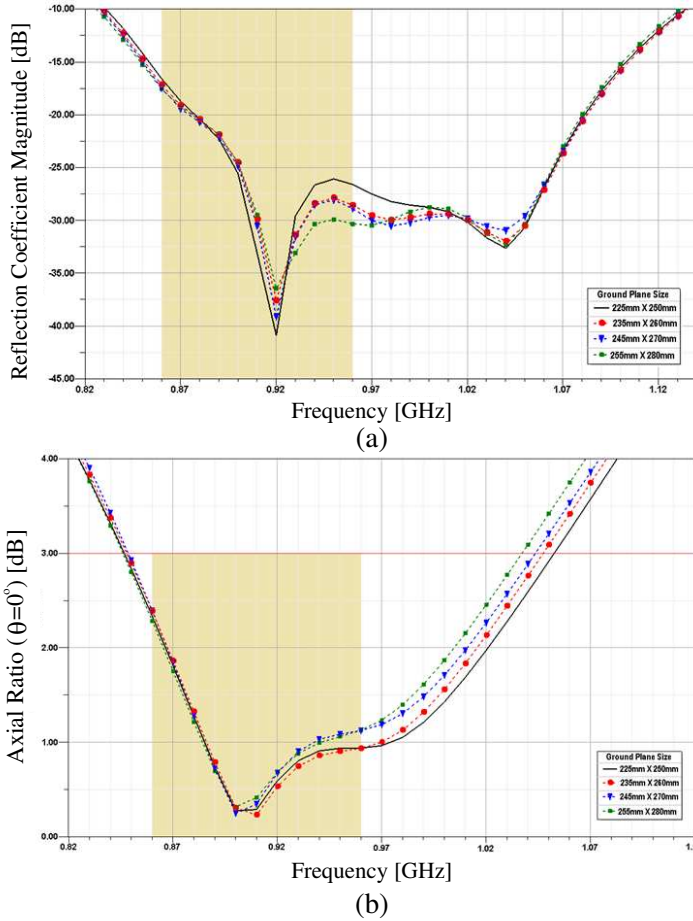


**Figure 5.** Parametric study results for different ground plane sizes. (a) Reflection coefficient magnitude (dB) vs. frequency (GHz), and (b) axial ratio (dB) at  $\theta = 0^\circ$  vs. frequency (GHz).

practically unchanged. The simulated AR for the proposed dimensions show a simulated band from 845 to 1052 MHz (22%) while the biggest case studied (255 mm  $\times$  280 mm) had an AR satisfying 3 dB from 845 to 1037 MHz (Figure 5(b)).

The length and width of the cross slot in the patch have a principal effect on tuning the maximum gain value (Figure 6) towards the center of the band while the matching band and axial ratio are slightly affected. The cross slot contributes to overall size reduction of the patch and thus efficient way for shifting the CP gain bandwidth.

Figures 6(a) and 6(b) show the CP gain for the width and length variations, respectively, while all other parameters remain constant.

A variation in the radius of the via holes ( $r_v$ ) may affect the inductive reactance of the antenna since it may affect the magnetic field surrounding the vias. Figures 7(a) and 7(b) show the reflection coefficient magnitude and axial ratio bandwidth versus frequency, respectively, as the via hole radius is increased in steps of 2 mm from 3 to 11 mm. Both bandwidths increase with the radius, which is a desirable effect, however, this variations in the antenna's impedance lead to a tendency of losing the matching and 3 dB axial ratio at the

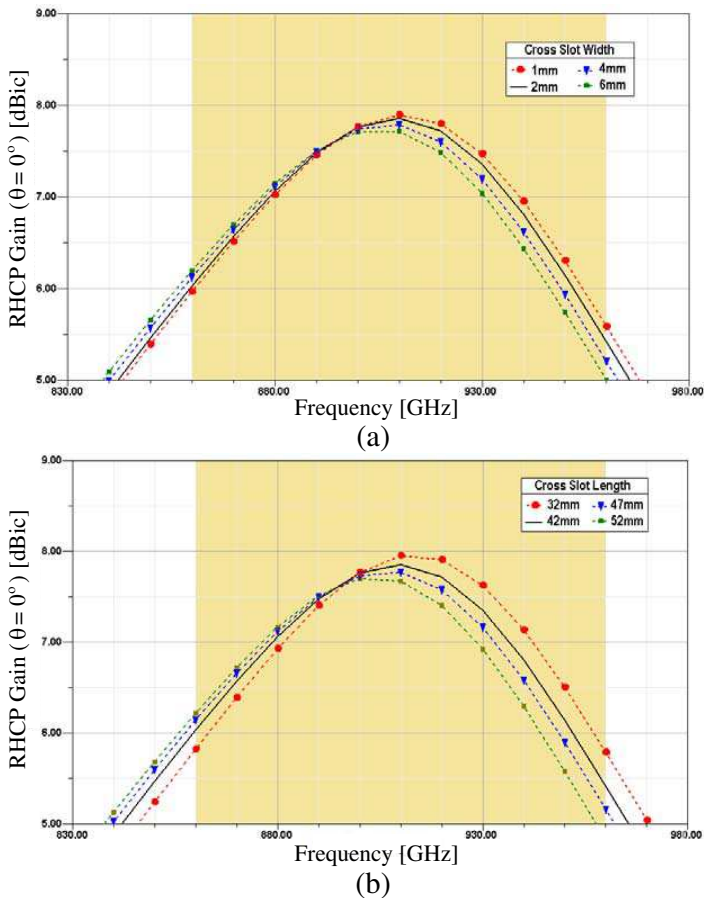


**Figure 6.** RHCP gain (dBic) versus frequency (MHz) parametric study results for different (a) cross-slot widths and (b) cross-slot lengths.

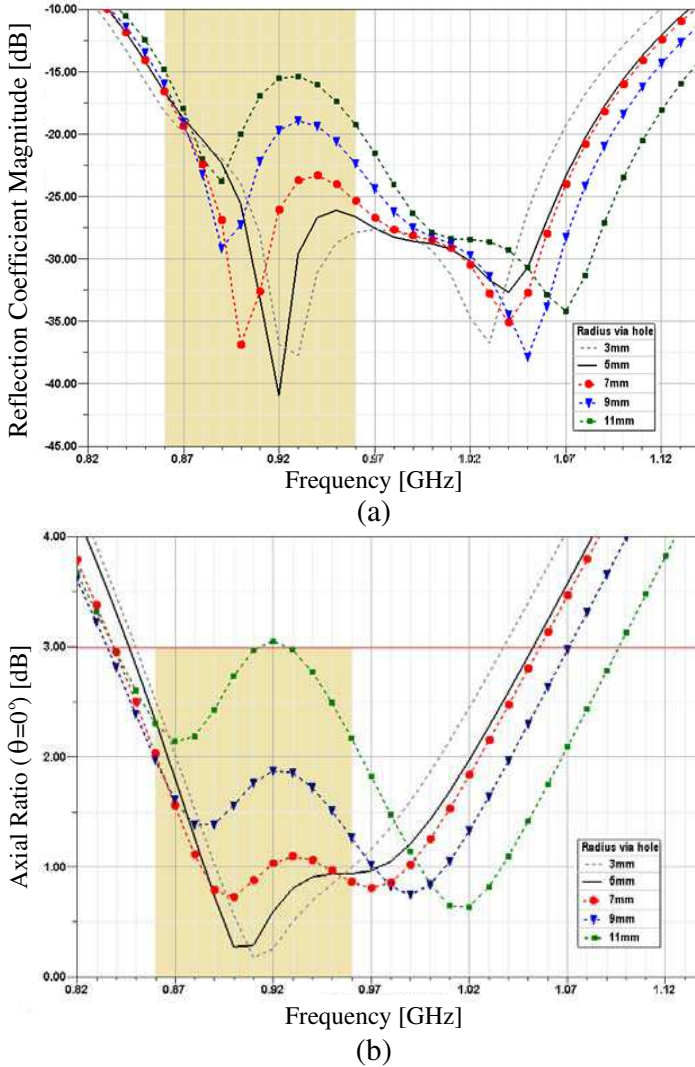


**Figure 7.** Antenna behavior as a function of the via holes radius. (a) Reflection coefficient magnitude (dB) vs. frequency (GHz), and (b) axial ratio (dB) at  $\theta = 0^\circ$  vs. frequency (GHz).

center of the target band. The maximum CP gain achieved suffers from a slight shift up in frequency as the radius increases but it remains around 7.8 dBic ( $\pm 0.2$  dBic) for all of the cases.

As the truncation of the corners (*a*) that are along the *y*-axis is increased, the length of the path traveled by the surface current

along the diagonals of the patch is modified, thus, shifting the resonant frequency of the two orthogonal modes that are responsible for the CP radiation pattern. In any case, the percentage bandwidth satisfying  $S_{11} \leq -10$  dB still remains within 30% covering the entire target band. For  $a = 10$  mm, the band covered is 822–1136 MHz (32%) while for  $a = 20$  mm ranges from 836 to 1126 MHz (29.6%) (Figure 8(a)). It is the axial ratio bandwidth that experiments a more significant change since it becomes broader towards higher end and closer to 0 dB at around 890 MHz as the truncation is made larger, which is a desirable

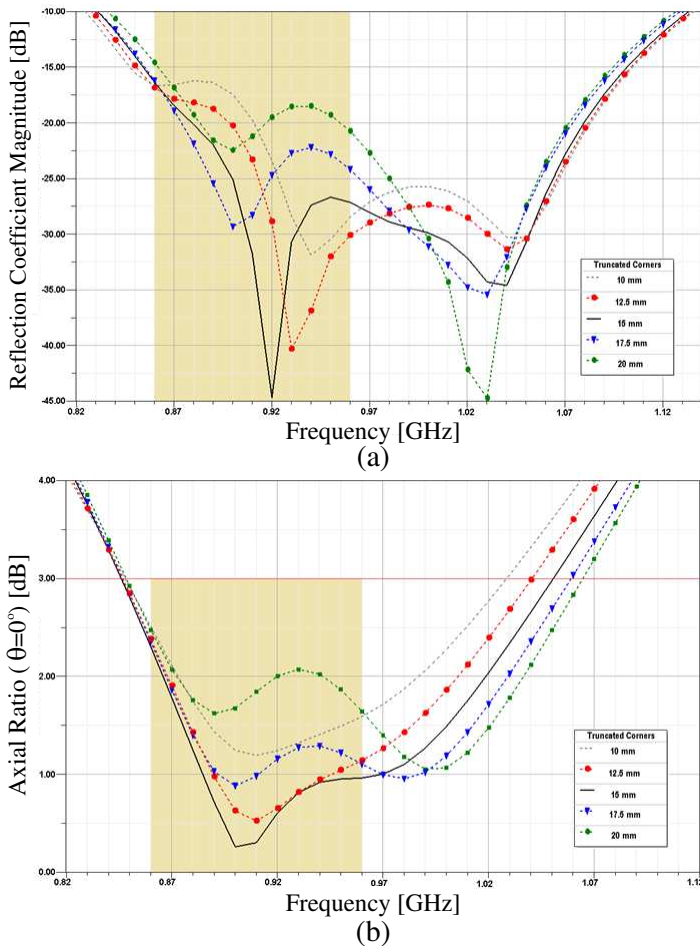


**Figure 8.** Effect of truncating the patch corners. (a) Reflection coefficient magnitude (dB) vs. frequency (GHz), and (b) axial ratio (dB) vs. frequency (GHz).

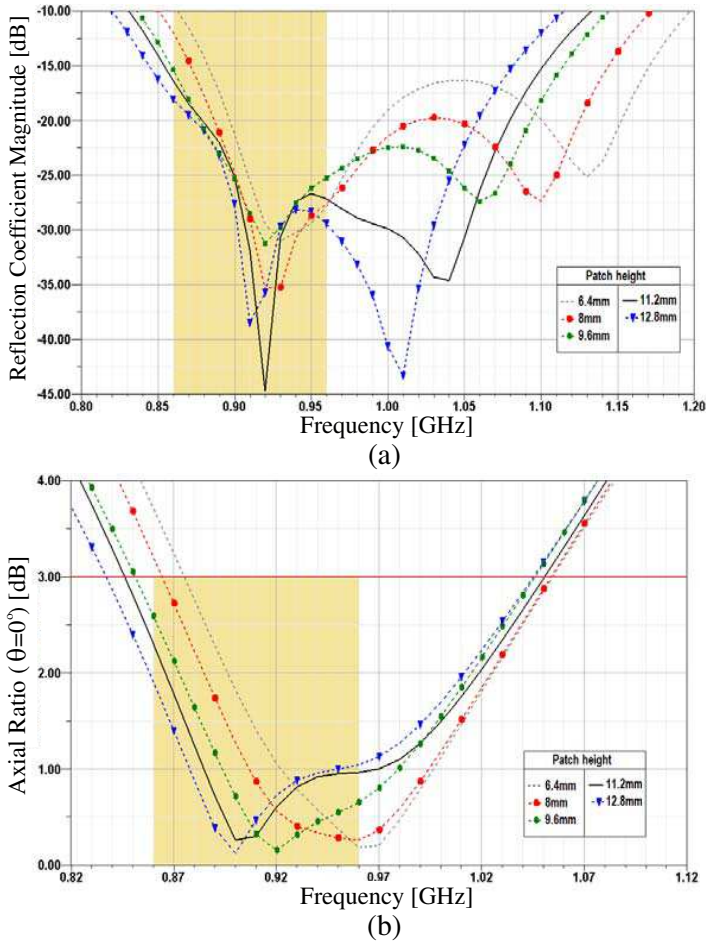


**Figure 9.** Parametric study for different patch heights. (a) Reflection coefficient magnitude (dB) vs. frequency (MHz), and (b) axial ratio ( $\theta = 0^\circ$ ) (dB) vs. frequency (GHz).

effect. However, further increasing the truncation beyond 20 mm leads to a degradation of the axial ratio bandwidth at the center of the band ( $AR > 3$  dB) (Figure 8(b)).

The variation in the height of the patch ( $h$ ) is a very sensitive parameter since the bandwidth of operation can be selected from correctly choosing this distance. It is well known that changing the substrate height in between the patch and ground plane will result in frequency shift while keeping the physical patch dimensions unchanged. This occurs due to the increase of the fringing fields at the edges of the

patch that extends its effective length causing a shift towards lower frequencies. This behavior can be clearly observed in Figures 9(a) and 9(b) for the matching and axial ratio bandwidths where the lower and higher ends shift by approximately the same amount w.r.t.  $S_{11} \leq -10$  dB and  $AR < 3$  dB as the height is increased in steps of 1.6 mm. Nevertheless, the matching band remains within 33% and 30% for  $h = 6.4$  and 12.8 mm, respectively, while the axial ratio bandwidth

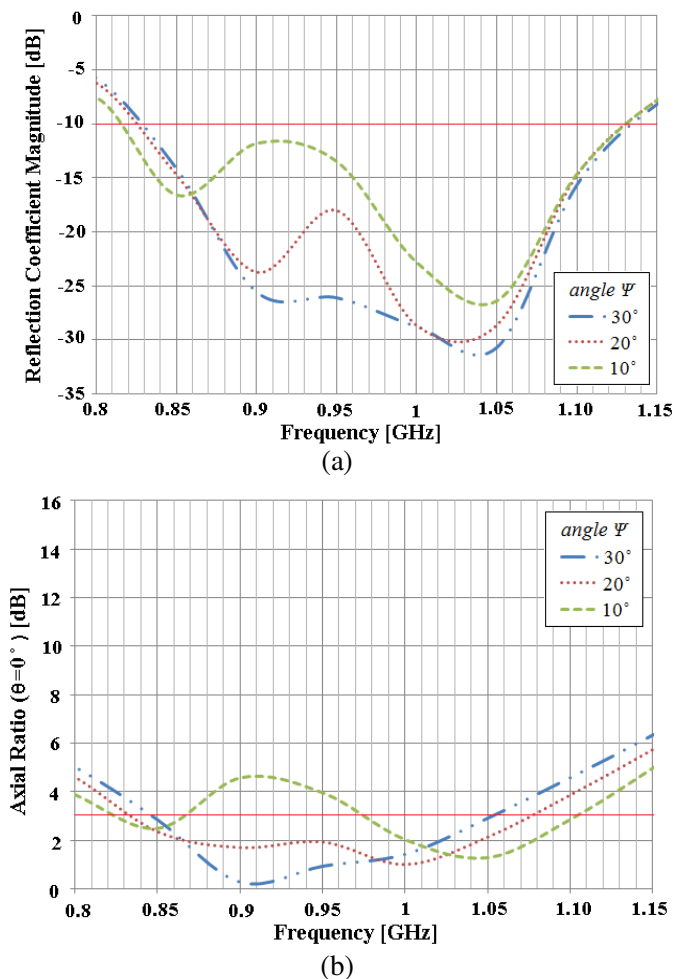


**Figure 10.** Parametric study results for different angle  $\Psi$ . (a) Reflection coefficient magnitude (dB) vs. frequency (GHz), and (b) axial ratio ( $\theta = 0^\circ$ ) (dB) vs. frequency (GHz).

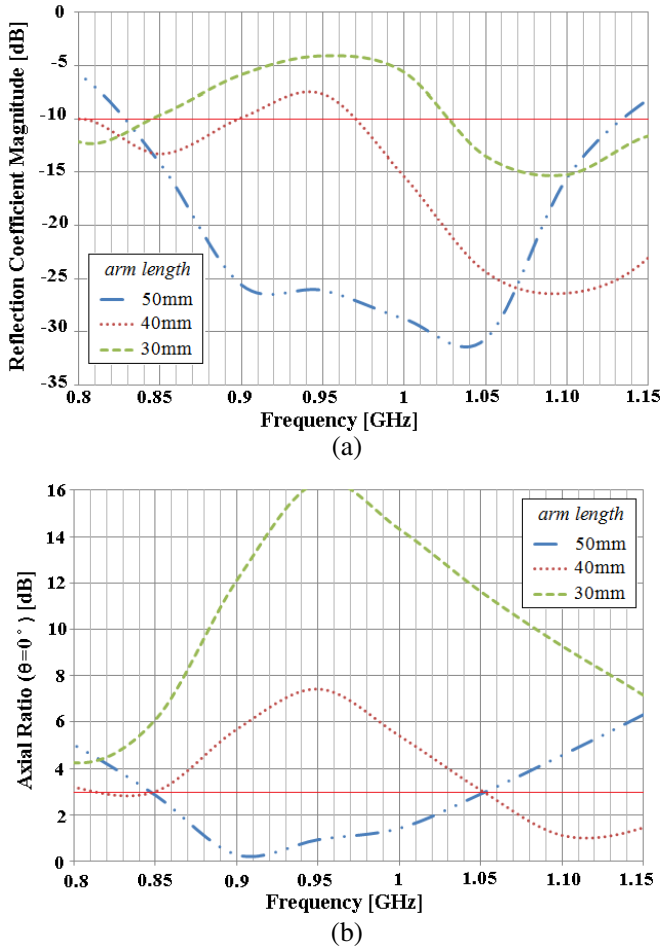


**Figure 11.** Parametric study results for different arm lengths. (a) Reflection coefficient magnitude (dB) vs. frequency (GHz), and (b) axial ratio ( $\theta = 0^\circ$ ) (dB) vs. frequency (GHz).

experiments a percentage bandwidth change from 17.7% to 22.3% for the same two heights.

Finding the best position to locate the feed points along the patch is an important parameter for obtaining a wideband axial ratio and impedance matching response. This position is controlled by the angle  $\Psi$  and the length of the output arms of the 3 dB coupler, both specified in Figure 2. Figures 10 and 11 show the antenna response when changing the feed location in terms of angle  $\Psi$  and the length of the

output arms of the 3 dB coupler. In Figure 10, the length of the output arms is kept constant to 50 mm (the final designated value) and angle  $\Psi$  varies for three different cases. In the case of Figure 11, the parameter angle  $\Psi$  is kept constant to  $30^\circ$  (the final designated value) while the length of the output arms varies for three different values. The selected final values for the model are angle  $\Psi = 30^\circ$  and length of the output arms = 50 mm.

### 3. EXPERIMENTAL VERIFICATIONS

The fabrication and measurement of the prototype antenna with chosen dimensions was completed in the Antenna and Microwave Laboratory (AML) at San Diego State University which has an Anritsu Vector

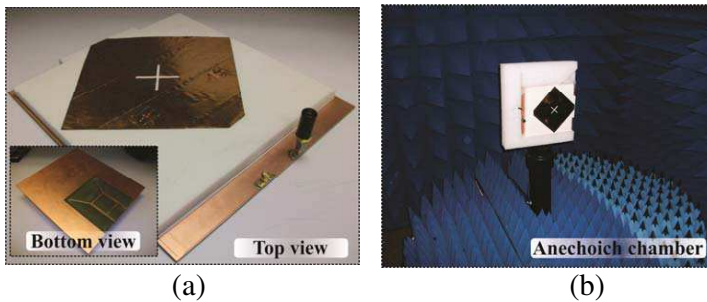


**Figure 12.** Fabricated prototype of the proposed RFID reader antenna. (a) Top and bottom view and (b) antenna under test (AUT) in chamber at AML, SDSU.

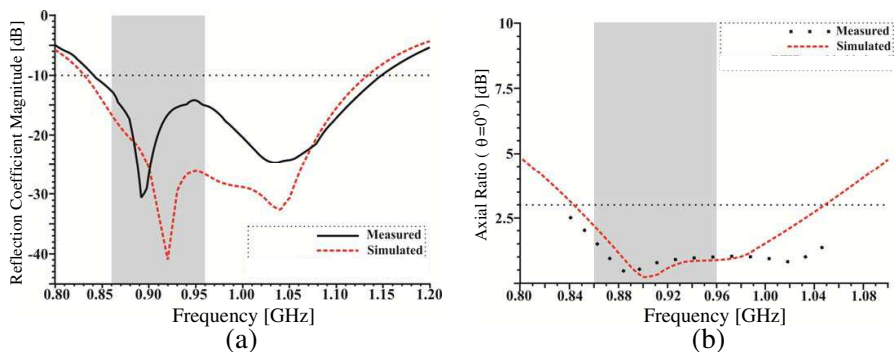


**Figure 13.** Measured and simulated (a) reflection coefficient ( $S_{11}$ ) magnitudes vs. frequency (GHz) and (b) axial ratio (dB) at broadside ( $\theta = 0^\circ$ ) vs. frequency (GHz).

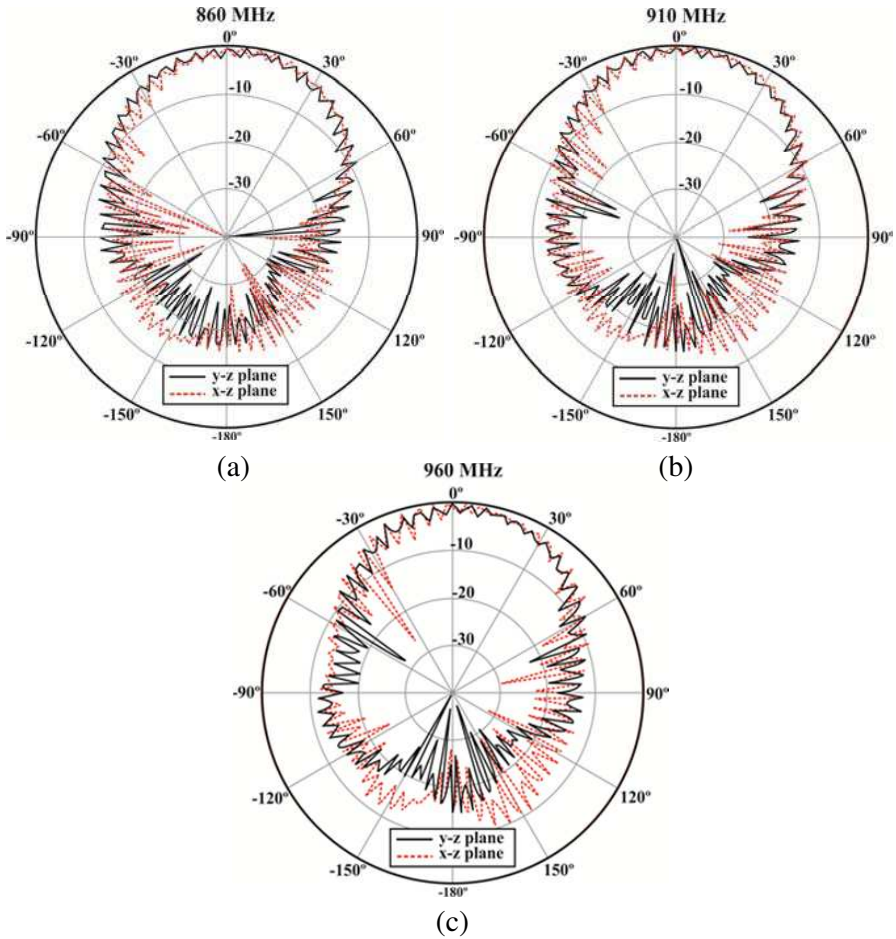


**Figure 14.** Measured normalized radiation patterns using a rotating linear source at frequencies within the UHF band (a) 860 MHz, (b) 910 MHz, and (c) 960 MHz.

Network Analyzer (VNA) model #37269D and an anechoic chamber of  $2.4 \times 2.4 \times 3.6$  meter<sup>3</sup> size with measurement system from Orbit F/R. A perspective and bottom view of the fabricated model is displayed on Figure 12(a). The hybrid network on FR-4 substrate was fabricated using LPKF milling machine including drilling of the via holes at the appropriate positions. The microstrip patch with the center cross-slots and truncated corners are sitting on a 11.2 mm thick layer of Cuming foam ( $\epsilon_r = 1.06$ ) substrate. Single sided adhesive copper tape is employed for the patch fabrication. A metallic wire was then soldered

inside the via holes to realize the via connections. Figure 12(b) shows the antenna under test (AUT) placed inside the anechoic chamber for radiation pattern measurements. For convenience in the fabrication process, the patch is sitting on an 11.2 mm thickness layer of foam ( $\epsilon_r = 1.06$ ). Figure 12(b) shows the antenna under test (AUT) placed inside the anechoic chamber for measurement of the radiation patterns.

The comparison of the measured and simulated reflection coefficients and axial ratio (AR) of the fabricated antenna are shown in Figures 13(a) and 13(b), respectively. The measured reflection coefficient magnitude (Figure 13(a)) covers a band from 840 to 1150 MHz with respect to (w.r.t)  $S_{11} \leq -10$  dB which yields a percentage bandwidth of 31.2% and agrees well with the simulated result of 830 to 1130 MHz (30.6%). The measured AR versus frequency at broadside angle ( $\theta = 0^\circ$ ) was obtained after post-processing of the rotating linear patterns following the technique described in [29]. The measured data (Figure 13(b)) exhibited AR better than 3 dB for the entire UHF RFID band and a percentage bandwidth better than 23% from 840 to 1050 MHz.

The normalized measured rotating linear radiation patterns are shown in Figures 14(a) to 14(c) for three different frequencies within the UHF band: 860 MHz, 910 MHz, and 960 MHz. A fairly wide AR beamwidth w.r.t.  $AR \leq 3$  dB of  $60^\circ$  is obtained for the three cases which suggest wide angular coverage for the RFID reader. The cross-polarization rotating linear components are not included with the plots because figure becomes too crowded. The presented patterns are directional and almost symmetric as expected for this antenna.

#### 4. CONCLUSIONS

A RFID reader antenna for worldwide UHF (840–960 MHz) applications is presented. The antenna consisted of a single layer microstrip patch fed using via through ground plane holes connected to a 3 dB quadrature branch line coupler printed on a low cost FR4 substrate material. The antenna showed impedance matching bandwidth from 840 to 1150 MHz and 3 dB AR bandwidth from 840 to 1050 MHz which meets and exceeds the worldwide UHF RFID band. Detailed parametric study results for the important antenna parameters, such as the radius of the via holes on the ground plane, truncation of the corners on the patch, location of the feed points on the patch, substrate or foam height for the patch, and branch line coupler construction parameters which helped arrive at the proposed novel antenna design, were discussed. The prototype antenna was fabricated and measured which showed good agreement between the simulated and measured data for

impedance matching and AR bandwidths along with the rotating linear based verification of the radiation patterns. The proposed antenna can serve as a good candidate for RFID fixed reader installations where a compromise of low cost, low volume and worldwide performance is required.

## ACKNOWLEDGMENT

This work was supported in part by National Science Foundation (NSF) under CAREER grant # ECCS-0845822. One of the authors would like to acknowledge Anup Kulkarni and Balamurugan Shanmugam for their considerable collaboration in the fabrication and measurement of the prototype.

## REFERENCES

1. Dobkin, D. M., *The RF in RFID: Passive UHF RFID in Practice*, Newnes, Burlington, MA, 2008.
2. Glover, B. and H. Bhatt, *RFID Essentials*, O'Reilly, Sebastopol, CA, 2006.
3. Balanis, C. A., *Antenna Theory Analysis and Design*, 3rd edition, Wiley Interscience, Hoboken, NJ, 2005.
4. Milligan, T., *Modern Antenna Design*, 2nd edition, IEEE Press, Hoboken, NJ, 2005.
5. Cushcraft Corporation, "Antenna polarization considerations in wireless communication systems," Manchester, 2002, <http://www.eie.fceia.unr.edu.ar/ftp/Antenas%20y%20Propagacion/Antenna-Polarization-14B32.pdf>.
6. Deavours, D. and D. Dobkin, "UHF passive tag antennas," *Microstrip and Printed Antennas: New Trends, Techniques, and Applications*, D. Guha and Y. M. Antar (eds.), 264–265, Wiley, United Kingdom, 2011.
7. Nikitin, P. V. and K. V. S. Rao, "Helical antenna for handheld UHF RFID reader," *IEEE International Conference on RFID*, 166–173, Orlando, FL, Apr. 2010.
8. Paret, D., *RFID at Ultra and Super High Frequencies Theory and Application*, 2nd edition, Wiley, United Kingdom, 2009.
9. Shin, D., P. Park, W. Seong, and J. Choi, "A novel dual-band circularly polarized antenna using a feeding configuration for RFID reader," *Proc. Int. Conf. on Electromagnetics in Advanced Applications*, 511–514, Torino, Italy, Sep. 2007.

10. Kwa, H. W., X. Qing, and Z. N. Chen, "Broadband single-fed single-patch circularly polarized antenna for UHF RFID applications," *IEEE Int. Symposium on Antennas and Propagation*, 1–4, San Diego, CA, USA, Jul. 2008.
11. Chen, X., G. Fu, S.-X. Gong, Y.-L. Yan, and W. Zhao, "Circularly polarized stacked annular-ring microstrip antenna with integrated feeding network for UHF RFID readers," *IEEE Antennas and Wireless Propagation Letters*, Vol. 9, 542–545, Jun. 2010.
12. Chung, H. L., X. Qing, and Z. N. Chen, "Broadband circularly polarized stacked patch antenna for UHF RFID applications," *IEEE Antennas and Propagation Society Int. Sym.*, 1189–1192, Honolulu, HI, USA, Jun. 2007.
13. Nassimudin, Y. S. B. and Z. N. Chen, "Broadband circularly polarized microstrip antenna for RFID reader applications," *Asia Pacific Microwave Conference*, 625–628, Singapore, Dec. 2009.
14. Wang, Z., S. Fang, S. Fu, and M. Fan, "Single-fed single-patch broadband circularly polarized antenna for UHF RFID reader applications," *2nd Int. Conf. on Industrial and Information Systems*, 87–89, Dalian, Jul. 2010.
15. Kim, D.-Z., H.-S. Tae, K.-S. Oh, M.-Q. Lee, and J.-W. Yu, "Helical reflector antenna with a wideband CP for RFID reader," *Asia Pacific Microwave Conference*, 1032–1035, Singapore, Dec. 2009.
16. Chen, Z. N., X. Qing, and H. L. Chung, "A universal UHF RFID reader antenna," *IEEE Transactions on Microwave Theory and Techniques*, Vol. 57, No. 5, 1275–1282, May 2009.
17. Garg, R., P. Bhartia, I. Bahl, and A. Ittipiboon, *Microstrip Antenna Design Handbook*, Artech House, Norwood, MA, 2001.
18. Albooyeh, M., N. Komjani, and M. Shobeyri, "A novel cross-slot geometry to improve impedance bandwidth of microstrip antennas," *Progress In Electromagnetics Research Letters*, Vol. 4, 63–72, 2008.
19. Lee, J. M., N. S. Kim, and C. S. Pyo, "A circular polarized metallic patch antenna for RFID reader," *Conf. on Communications Asia-Pacific*, 116–118, Perth, WA, Oct. 2005.
20. Pozar, D. M., *Microwave Engineering*, 3rd edition, Wiley, Hoboken, NJ, 2005.
21. Lin, Y.-F., H.-M. Chen, S.-C. Kao, and C.-Y. Lin, "Adjustable axial ratio of single-layer circularly polarized patch antenna for portable RFID reader," *Electronics Lett.*, Vol. 45, No. 6, Mar. 2009.

22. Balanis, C. A., *Modern Antenna Handbook*, Chapter 4, John Wiley & Sons Inc., USA, 2008.
23. Qing, X. and N. Yang, "2.45 GHz circularly polarized RFID reader antenna," *Ninth Int. Conf. on Communications Systems*, 612–615, Singapore, Sept. 2004.
24. Yi, M., S. Li, H. Liu, and W. Hong, "A novel antenna with a feed networks for RFID reader at ultra high frequency," *11th IEEE Int. Conf. on Communication Systems*, 801–804, Singapore, Nov. 2008.
25. Lin, P.-J., H.-C. Teng, Y.-J. Huang, and M.-K. Chen, "Design of patch antenna for RFID reader applications," *3rd Int. Conf. on Anti-counterfit, Security, and Identification in Communication*, 193–196, Hong Kong, China, Aug. 2009.
26. Wang, Z., S. Fang, S. Fu, and X. Li, "Circularly polarized antenna with U-shaped strip for RFID reader operating at 902–928 MHz," *Int. Sym. on Signals Systems and Electronics*, 1–3, Nanjing, China, Sept. 2010.
27. Mireles, E. and S. K. Sharma, "A broadband microstrip patch antenna fed through vias connected to a 3dB quadrature line coupler for worldwide UHF RFID reader applications," *IEEE Antennas and Propagation Society International Symposium (IEEE AP-S)*, Spokane, Washington, USA, Jul. 3–8, 2011.
28. Pozar, D. M., "Microstrip antennas," *Proc. of the IEEE*, Vol. 80, No. 1, 79–91, Jan. 1992.
29. Kraus, J. D. and R. Markhefka, *Antennas for All Applications*, 3rd edition, McGraw Hill, New York, NY, 2002.